Materials Research Bulletin 55 (2014) 13–18

Contents lists available at ScienceDirect

Materials Research Bulletin

journal homepage: www.elsevier.com/locate/matresbu

Self-assembled highly crystalline TiO_2 mesostructures for sunlight-driven, pH-responsive photodegradation of dyes

Xinyi Zhang [a,b,*], Jianfeng Yao [c], Dan Li [c], Xiaodong Chen [c], Huanting Wang [c], Leslie. Y. Yeo [d], James. R. Friend [b,d,*]

[a] School of Chemistry, Monash University, Clayton, VIC 3800, Australia
[b] Melbourne Centre for Nanofabrication, Clayton, VIC 3800, Australia
[c] Department of Chemical Engineering, Monash University, Clayton, VIC 3800, Australia
[d] Micro/Nanophysics Research Laboratory, RMIT University, Melbourne, VIC 3000, Australia

ARTICLE INFO

Article history:
Received 16 July 2013
Received in revised form 26 December 2013
Accepted 31 March 2014
Available online 04 April 2014

Keywords:
A. Semiconductor
A. Oxide
C. Transmission electron microscopy (TEM)
D. Crystal structure
D. Catalytic properties

ABSTRACT

The development of new strategies and photocatalytic materials for practical environmental solutions remains a great challenge, particularly due to the large energy demands associated with various remediation processes. In this paper, we report the fabrication of self-assembled ordered mesoporous TiO_2 with highly crystalline anatase structures as well as high surface area, and characterize their photocatalytic performance on the degradation of three typical dyes, including anionic methyl orange, cationic methylene blue, and neutral rhodamine B driven merely by sunlight. The results show that the dye photodegradation strongly depends on the charging state of both mesoporous TiO_2 surface and dyes, which can be adjusted by the pH value of the solutions. Such charge-dependent photocatalytic functionality of mesoporous TiO_2 can thus be exploited for highly efficient and selective dye photodegradation.

1. Introduction

Dyes are common across many industries—including printing, textile, pulp and paper, and leather processing—to color products to suit customer desires, generating substantial amounts of dye wastewater that is harmful to the environment, hazardous to human health, and difficult to degrade by natural means. Their use remains problematic, an anachronism remaining among the many chemicals produced and used via sustainable processes developed in recent years. Numerous treatment technologies have been developed to treat dye wastewater, from physico-chemical to biological processes [1–6]. Among these, the solar energy-driven photodegradation of dyes in aqueous solutions has gained considerable attention due to practical and fundamental benefits alike in recognition of the impact dye-laden waste has on the environment [7–10]. Semiconductor-based photocatalysis has attracted particular attention as a suitable "green" technology for this purpose because of its chemical stability and favorable energy band structure. TiO_2 is considered to be one of the best material candidates for photovoltaic and photocatalytic devices in this application; its nanoparticles possess superior photocatalytic efficiency over the bulk phase and the photocatalytic activity of such nanoparticles have been extensively investigated [11–13]. However, intrinsic limitations prevent further improvement in the photocatalytic process in TiO_2 nanoparticles. Illuminated TiO_2 nanoparticles behave as short-circuited electrodes: the interfacial charge transfer competing with the charge recombination between the charge carriers is a major problem in photocatalysis and is a limiting factor in improving the photocatalytic efficiency [14]. There are further drawbacks: nanoparticles tend to aggregate, are difficult to separate and recover from solution, and the environmental impact of such nanoparticles remains an open question, greatly limiting their practical use in many commercial applications. The significant need remains, therefore, for another approach and alternative materials to solve these challenging problems inherent in TiO_2 and in using them in a nanoparticle morphology.

So far, little information is available on the reaction mechanisms involved in the photocatalytic degradation of dyes and on the identification of major transient intermediates which have been more recently recognized as very important aspects of these processes, especially from the viewpoint of practical application [15–17]. As the charging states of both dye and photocatalyst play

* Corresponding author. Tel.: +61 3 9902 4619; fax: +61 3 9905 4597.
E-mail addresses: xinyi.zhang@monash.edu (X. Zhang), james.friend@rmit.edu.au (J.R. Friend).

http://dx.doi.org/10.1016/j.materresbull.2014.03.036
0025-5408/

crucial roles in the photodegradation process, investigating the prior adsorption of dyes in addition to the interactions between the dyes and the catalyst surface is crucially important to develop superior photocatalysts for efficient dye degradation. In comparison with TiO_2 nanoparticles, highly structured mesoporous TiO_2 formed using evaporation-induced self-assembly is of considerable interest [18–20]. The advantage of this technique lies in the possibility of "tuning" the symmetry of the mesostructure by adjusting the composition of the initial solution and the preparation condition [21–23]. Further, the mesoporous morphology avoids the myriad practical drawbacks of nanoparticles. To the best of our knowledge, there is no study to date on the pH-responsively selective photocatalytic activity of ordered mesoporous TiO_2. Here, we report the fabrication of self-assembled highly crystalline ordered mesoporous TiO_2 and investigate the sunlight-driven photocatalytic activity of the mesoporous TiO_2. The results show that the adsorption of dyes on the mesoporous TiO_2 surface strongly depends on the pH value of the dye solution in addition to the charging state of the dyes, and that these factors in turn have a crucial effect on the photocatalytic performance of the mesoporous TiO_2.

2. Experimental

Mesoporous TiO_2 was synthesized by using a mixture of poly (ethylene oxide)-*b*-poly(propylene oxide)-*b*-poly(ethylene oxide) copolymer (P123), ethanol, concentrated HCl, and tetrabutyl titanate (TBT) [24]. The mass ratio of P123/TBT/EtOH/HCl was 1:2.8:30:2. For a typical synthesis, 1.0 g of P123 was dissolved in 30 g of ethanol, and then 2 g of concentrated HCl was slowly added with stirring. Then 2.8 g of TBT was added, and the solution was stirred for 4 h. The resulting solutions were transferred into Petri dishes and subsequently sealed and aged at room temperature for 1 week. Then the samples were calcined at 400 °C in air for 2 h with a 1 °C min^{-1} temperature ramp to obtain the mesoporous TiO_2 thin films with thickness of about 2 μm. All chemical reagents used in this study were of analytical grade and were supplied by Sigma–Aldrich (Australia). Nitrogen adsorption–desorption experiments were performed at 77 K with a Micromeritics ASAP 2020MC. The samples were degassed at 300 °C for 5 h prior to measurement. The pore volume was estimated from the desorption branch of the isotherm at $P/P_o = 0.98$ assuming complete pore saturation. The morphology and microstructure of the mesoporous TiO_2 were investigated using an X-ray diffractometer (XRD, PW1140/90) with CuKa radiation (25 mA and 40 kV), and a transmission electron microscope (TEM, JEOL-2011).

Three typical dyes including rhodamine B (RB), methyl orange (MO), and methylene blue (MB) were studied for photodegradation. The molecule structures of the dyes are shown in Fig. 1. The concentrations of the dye solutions were 50 mg/L. 10 mg of the mesoporous TiO_2 samples were added into 20 mL dye solution and the muddy solution was dispersed with an ultrasonic instrument for 30 min, and then irradiated by sunlight. The temperature was in the range of 22–26 °C and the average sunlight intensity was about 6.5 kW h m^{-2}. The pH of the samples was adjusted by using 0.1 mol/L HCl or 0.1 mol/L NaOH. After the photocatalytic experiment, the remaining dye solutions were collected and analyzed. A UV-240 UV–vis spectrometer was used to record the change of the absorbance of the dye solution.

3. Results and discussion

The TiO_2 mesostructures were formed using the evaporation induced self-assembly (EISA) approach, which has been established as an efficient process for the preparation of mesostructured oxide with controlled morphologies [24]. The wide-angle X-ray diffraction pattern of the sample is shown in Fig. 2a. The main diffraction peaks correspond to the tetragonal structure of anatase TiO_2. Fig. 2b exhibits the small angle X-ray diffraction spectrum, clearly showing the principle diffractional peak (1 0 0) and suggesting a well-defined hexagonal mesostructure. The N_2 sorption isotherms of mesoporous TiO_2 show type-IV curves with clear condensation steps, indicating uniform mesopores (Fig. 2c). The Langmuir surface area which is calculated from nitrogen sorption results to be 172.2 m^2/g. Fig. 2d shows the derived pore size distributions. The pore size distributions of the samples are observed to be narrow and the corresponding peak is located at about 4.8 nm, confirming the formation of the mesostructure [25].

The mesostructure of the TiO_2 was further investigated by transmission electron microscopy (TEM). The TEM images of the ordered mesoporous structure of the TiO_2 are displayed in Fig. 3. As shown in Fig. 3a, the cross-sectional view of the mesoporous TiO_2

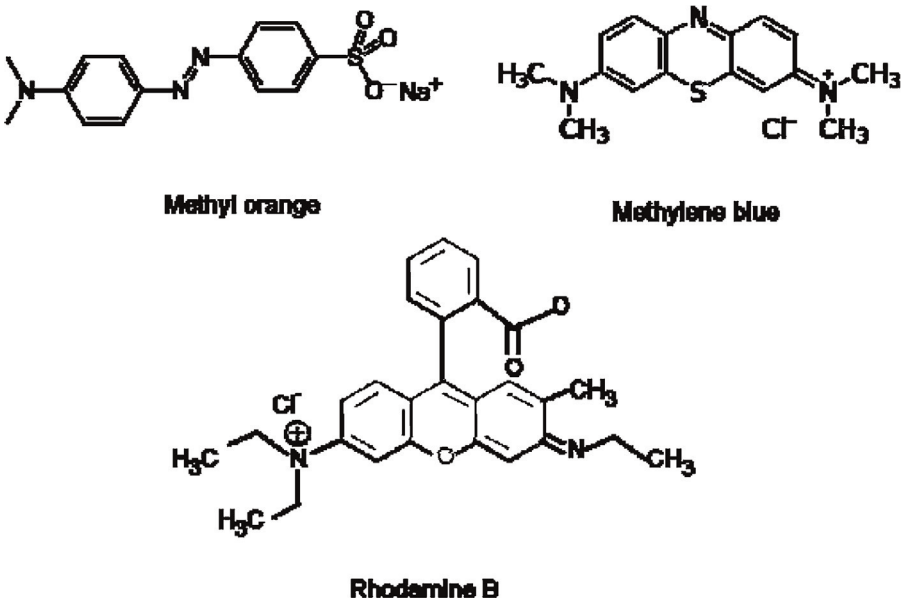

Fig. 1. The molecule structures of dyes.

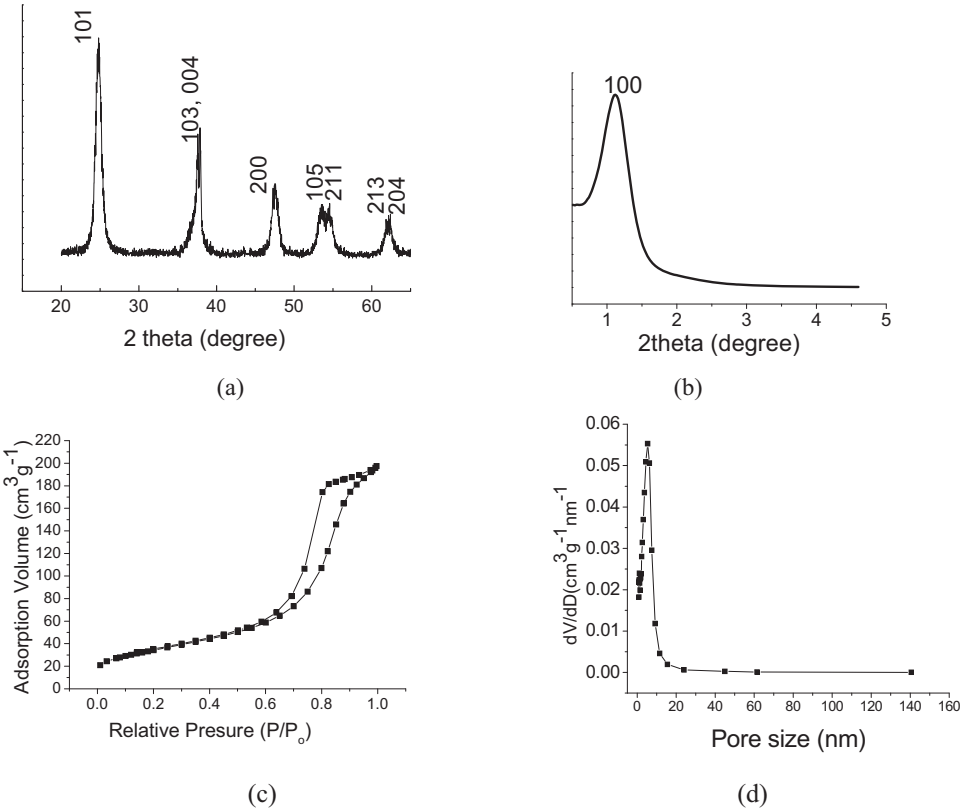

Fig. 2. (a) Wide-angle and (b) small-angle XRD spectrum. (c) The N_2 sorption isotherm and (d) pore size distribution of mesoporous TiO_2.

exhibits parallel cylindrical channels. Fig. 3b shows the plain view of the mesoporous TiO_2, where ordered hexagonally-organized mesopores with pore sizes of 3–5 nm can be clearly observed. The inset in Fig. 3b shows the corresponding electron diffraction (ED) pattern and the strong and continuous rings can be indexed as the anatase TiO_2 structure, which is in accordance with the X-ray diffraction (XRD) analysis. The high-resolution TEM (HRTEM) images of the mesopore wall in the mesoporous TiO_2 are displayed in Fig. 3c and d wherein the well-recognized lattice spacings of 0.35 and 0.19 nm correspond to the anatase (1 0 1) and (2 0 0)

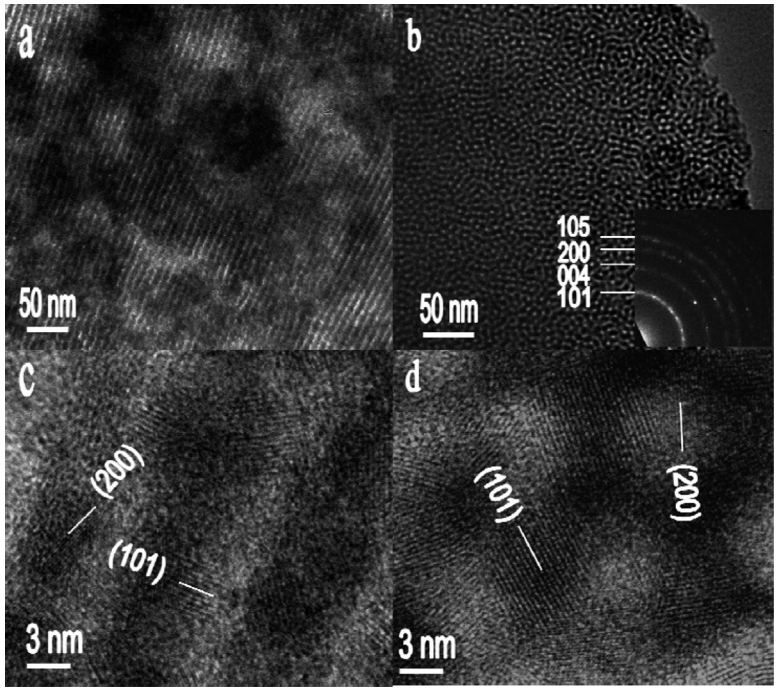

Fig. 3. TEM images show (a) the cross section, and, (b) plane view and HRTEM images show (c) the cross sectional view, and, (d) the plane view of the mesoporous TiO_2.

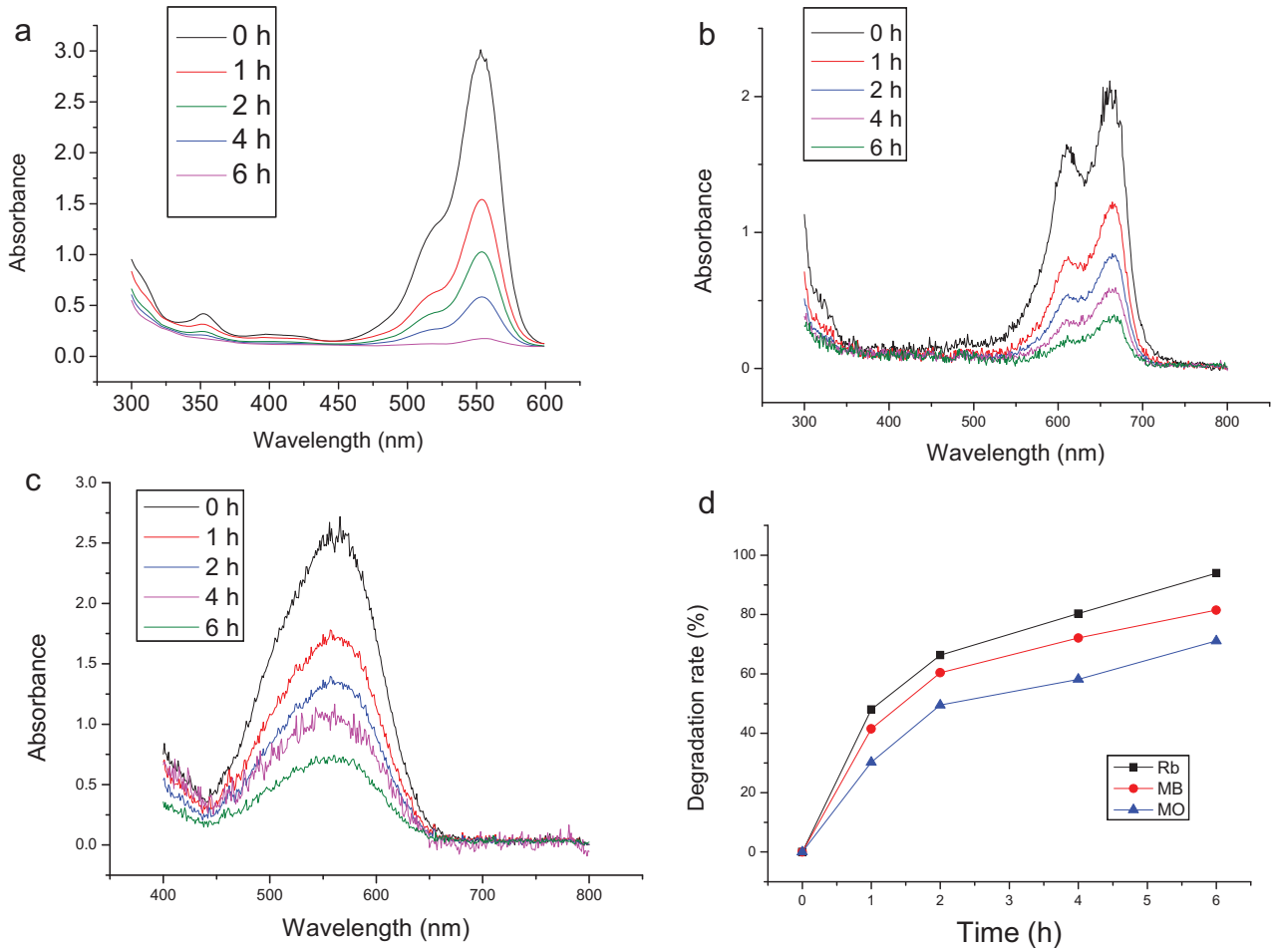

Fig. 4. The adsorption spectra of (a) RB, (b) MB, and (c) MO dyes at various irradiation times on mesoporous TiO_2, and (d) the photocatalytic degradation rate of the dyes on mesoporous TiO_2 as a function of irradiation time in neutral solutions.

atomic planes, respectively. The interpore distance is about 6 nm, which is consistent with the lattice parameter (~6 nm) of the hexagonal mesophase of the P123 liquid crystal.

Fig. 4 shows the sunlight-driven photocatalytic degradation of dyes on mesoporous TiO_2 in neutral solutions (pH 6.5). The adsorption spectra of RB, MB, and MO dyes at various irradiation times on mesoporous TiO_2 are shown in Fig. 4a, b, and c, respectively. As illustrated in Fig. 4d, the photocatalytic degradation of different dyes on mesoporous TiO_2 is quite different (Fig. 4d). The degradation rates of dyes are in the order of MO < MB < RB. Among them, the highest activity with a degradation rate of around 51% was obtained for RB after 1 h of sunlight irradiation. The degradation mechanism of dyes under sunlight irradiation is clearly different from that under UV irradiation. During UV irradiation, electron (e^-)–hole (h^+) pairs are generated and are capable of initiating oxidation and reduction reactions on the surface of TiO_2 [26,27]. The dyes are aromatic compounds containing aryl rings which have delocalized electron systems. These are responsible for the absorption of electromagnetic radiation of varying wavelengths; the cleavage of conjugated chromophore structures occuring during the photodegradation process. Under sunlight irradiation, electron transfer to the TiO_2 surface is achieved mainly through the extraction of electrons from excited dyes to the conduction band of TiO_2 directly or photogenerated holes from the dyes to the valence band of TiO_2, respectively. The dyes with labile organic functional groups are more easily to be excited and converted to the dye radicals that subsequently undergo degradation. The dye radicals readily react with hydroxyl ions undergoing oxidation or interacts effectively with $O_2^{\cdot -}$, $HO_2^{\cdot -}$ or $HO^{\cdot -}$ species to yield intermediates that ultimately lead to CO_2. The mechanism of solar light-induced photocatalytic degradation of dyes is schematically presented in Fig. 5. In neutral solutions, the differences in the ease of formation of the dye radical and the stability of the aryl rings should be

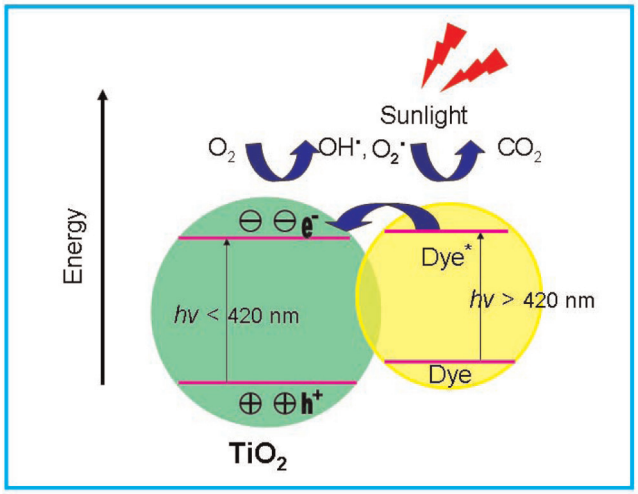

Fig. 5. Schematic illustration of sunlight-driven photocatalytic mechanism of dye degradation on mesoporous TiO_2.

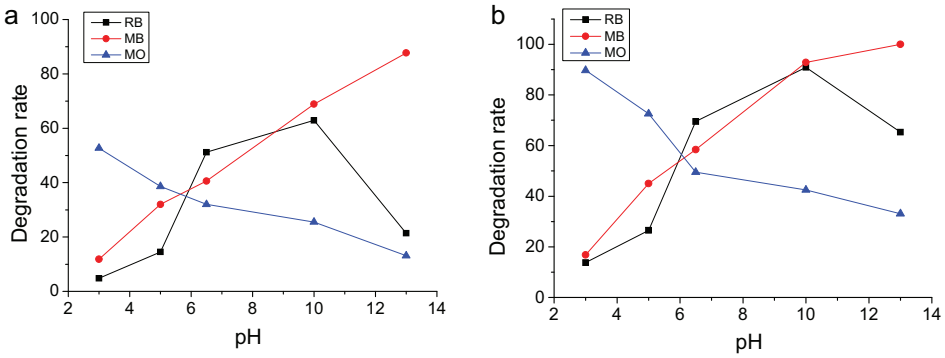

Fig. 6. The sunlight-driven photocatalytic degradation of dyes on mesoporous TiO_2 as a function of pH after (a) 1 h and (b) 2 h of irradiation.

mainly responsible for the difference in the degradation rates among the dyes [28,29]. As shown in Fig. 6, the photocatalytic performance of mesoporous TiO_2 is strongly dependent on the pH of the dye solutions. The photodegradation rate of MO is observed to decrease with increasing pH, whereas the photodegradation rate of MB is seen to increase with increasing pH. In contrast, the photodegradation rate of RB also increases with increasing pH though its degradation rate nevertheless drops significantly in strong alkaline solution. The adsorption of dyes on the surface of catalysts is indispensable for photocatalytic degradation. Therefore, the charging state of the dyes and catalyst surface should be taken into consideration. Fig. 7 shows the ζ-potential of mesoporous TiO_2 surface in aqueous solution with different pH values. The TiO_2 surface is positively charged at pH 8 or below and becomes negatively charged upon increasing the pH. Since MO is an anionic dye containing sulphonate group whereas MB is a cationic dye containing amino groups, it can then be inferred that the cationic dye MB prefers to adsorb on the catalyst surface at pH above 8, while the anionic dye MO prefers to adsorb on the catalyst surface at pH lower than 8. The charging states of both the TiO_2 and dyes change when the pH of the solution changes. The increase of pH decreases the positive charging of the TiO_2 surface. For the anionic MO dye, the increase of pH then decreases the attraction between anionic MO molecules and the TiO_2 surface, especially on negatively charged TiO_2 surfaces at high pH. Besides, the increase in pH also leads to an increase in the competition between OH^- and MO during their adsorption onto the catalyst surface. These factors then lead to the decrease of degradation rates of MO with increasing pH. For MB, on the other hand, the increase in pH decreases the repulsion between the cationic MB molecules and the TiO_2 surface whilst also enhancing the base-catalyzed demethylation of MB [30]. Therefore, the degradation rate of MB is seen to increase with increasing pH. RB, in contrast, is positively charged, neutral, and negatively charged in the pH range below 6.0, 6.0 to 10.8, and above 10.8, respectively [31]. At low pH, the situation for RB is similar to that for MB, and hence the degradation rate of RB is very low because of the difficulty of the adsorption. An increase in pH, however, decreases the positive charging of both the TiO_2 surface and RB. The degradation of neutral RB molecules then suggests that the adsorption of RB can be achieved via hydrogen bonding or van der Waals forces in neutral solution. Conversely, both TiO_2 surface and RB molecules are negatively charged at strong alkaline solution (pH > 10.8) and therefore the repulsion between the TiO_2 surface and anionic RB molecules suppresses the adsorption and hence the degradation of RB.

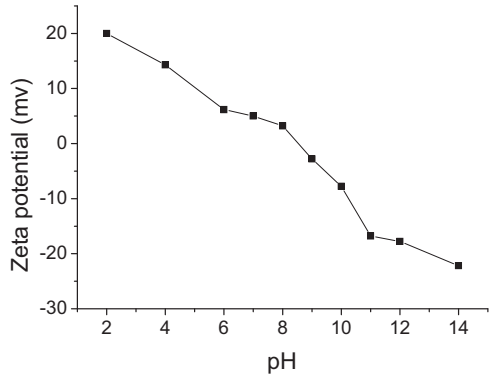

Fig. 7. The ζ-potential of the mesoporous TiO_2 as a function of pH.

4. Conclusions

In conclusion, ordered mesoporous TiO_2 with highly crystalline walls and large surface area has been prepared and characterized. The sunlight-driven photocatalytic degradation of various dyes on mesoporous TiO_2 and the role of pH in the photocatalytic degradation process was then systematically investigated. We demonstrate that the photocatalytic activity of mesoporous TiO_2 is strongly pH-responsive, and can therefore be controlled by adjusting the pH of the aqueous solutions. All of the dyes were shown to be effectively photocatalytic degraded on mesoporous TiO_2 by selecting a suitable pH range. This work therefore shows the potential of heterogeneous photocatalysis to decontaminate dye wastewater and opens up a new way for designing sunlight-driven photocatalysts for environmental remediation.

Acknowledgements

This work was supported by the Australian Research Council (ARC) (Grant No.: DP120104334) and Monash University. This work was performed in part at the Melbourne Centre for Nanofabrication (MCN) in the Victorian Node of the Australian National Fabrication Facility (ANFF).

References

[1] S.C. Yan, Z.S. Li, Z.G. Zou, Langmuir 26 (2010) 3894–3901.
[2] Y.F. Xie, D.Y. Qin, D.L. Wu, X.F. Ma, Chemical Engineering Journal 168 (2011) 959–963.
[3] A. Zille, P. Ramalho, T. Tzanov, R. Millward, V. Aires, M.H. Cardoso, M.T. Ramalho, G.M. Gübitz, A. Cavaco-Paulo, Biotechnology Progress 20 (2004) 1588–1592.
[4] Y.S. Al-Degs, M.I. El-Barghouthi, A.H. El-Sheikh, G.M. Walker, Dyes Pigments 77 (2008) 16–23.
[5] N.K. Amin, Journal of Hazardous Materials 165 (2009) 52–62.
[6] M. Arami, N.Y. Limaee, N.M. Mahmoodi, Journal of Colloid and Interface Science 288 (2005) 371–376.
[7] V.M. Correia, T. Stephenson, S.J. Judd, Environmental Technology 15 (1994) 917–929.

[8] I.K. Konstantinou, T.A. Albanis, Applied Catalysis B: Environment 49 (2004) 1–14.
[9] A. Houas, H. Lachheb, M. Ksibi, E. Elaloui, C. Guillard, J.M. Hermann, Applied Catalysis B: Environment 31 (2001) 145–157.
[10] K. Tanaka, K. Padermpole, T. Hisanaga, Water Research 34 (2000) 327–333.
[11] W. Zhao, Y.L. Sun, F.N. Castellano, Journal of the American Chemical Society 130 (2008) 12566–12567.
[12] X.B. Chen, L. Liu, P.Y. Yu, S.S. Mao, Science 331 (2011) 746–750.
[13] J.K. McCusker, Science 293 (2001) 1599–1601.
[14] W.A. Zeltner, M.A. Anderson, The use of nanoparticles in environmental applications, in: E. Pelizzetti (Ed.), Fine Particles Science and Technology, Kluwer Academic Publishers, Dordrecht, the Netherlands, 1996, pp. 643–656.
[15] F. Zhang, J. Zhao, T. Shen, H. Hidaka, E. Pelizzetti, N. Serpone, Applied Catalysis B: Environment 15 (1998) 147–156.
[16] F. Chen, Y. Xie, J. Zhao, G. Lu, Chemosphere 44 (2001) 1159–1168.
[17] G.A. Epling, C. Lin, Chemosphere 46 (2002) 561–570.
[18] C.T. Kresge, M.E. Leonowicz, W.J. Roth, J.C. Vartuli, J.S. Beck, Nature 359 (1992) 710–712.
[19] M.M. Turnbull, C.P. Landee, Science 298 (2002) 1723–1724.
[20] D. Zhao, J. Feng, Q. Huo, N. Melosh, G.H. Fredrickson, B.F. Chmelka, G.D. Stucky, Science 279 (1998) 548–552.
[21] S.S. Soni, M.J. Henderson, J.F. Bardeau, A. Gibaud, Advanced Materials 20 (2008) 1493–1498.
[22] P.G. Hoertz, T.E. Mallouk, Inorganic Chemistry 44 (2005) 6828–6840.
[23] S. Sajjad, S.A.K. Leghari, F. Chen, J.L. Zhang, European Journal of Chemistry 16 (2010) 13795–13804.
[24] H.S. Yun, K. Miyazawa, H.S. Zhou, I. Honma, M. Kuwabara, Advanced Materials 13 (2001) 1377–1380.
[25] K. Hou, B.Z. Tian, F.Y. Li, Z.Q. Bian, D.Y. Zhao, C.H. Huang, Journal of Materials Chemistry 15 (2005) 2414–2420.
[26] D. Friedmann, C. Mendive, D. Bahnemann, Applied Catalysis B: Environmental 99 (2010) 398–406.
[27] A. Mills, D. Worsley, R.H. Davies, Journal of the Chemical Society, Chemical Communications (1994) 2677.
[28] Takizawa, T. Watanabe, K. Honda, Journal of Physical Chemistry 82 (1978) 1391–1396.
[29] J. Oakes, P. Gratton, Journal of the Chemical Society, Perkin Transactions 2 (1998) 2563–2568.
[30] K. Bergmann, C.T. O'Konski, Journal of Physical Chemistry 67 (1967) 2169–2177.
[31] Y.J. Oh, T.C. Gamble, D. Leonhardt, C.H. Chung, S.R.J. Brueck, C.F. Ivory, G.P. Lopez, D.N. Petsev, S.M. Han, Lab on a Chip 8 (2008) 251–258.